Organic Chemistry Frontiers

ARTICLE

Dibenzopyridoimidazocinnolinium cations: a new family of light-up fluorescent DNA probes

Received 00th January 20xx,
Accepted 00th January 20xx

DOI: 10.1039/x0xx00000x

www.rsc.org/

Pedro Bosch,[a] David Sucunza,*[,a] Francisco Mendicuti,[b] Alberto Domingo[c] and Juan J. Vaquero*[,a]

Steady-state and time-resolved fluorescence, circular dichroism and molecular modelling techniques have been applied to a new family of weakly fluorescent dibenzopyridoimidazocinnolinium derivatives whose fluorescence intensity increases significantly (larger than ×3.5) upon DNA addition. The synthesis of these azonia cations, which bind to DNA by intercalation, was carried out using a Westphal condensation and a Suzuki cross coupling reaction as key steps. A live-cell staining analysis by confocal microscopy imaging was also performed and showed the capacity of these new compounds for active uptake and accumulation by living cells, with complex patterns of intracellular distribution observed.

Introduction

The development of fluorescent probes whose emission intensity is enhanced by complex formation with DNA ('light-up probes') has attracted widespread attention due to their applications in analytical biochemistry and medicine.[1] Several dyes that fulfill this characteristic have been developed in recent years.[2] Commonly, DNA-binding molecules interact with this biomacromolecule via three different modes, namely intercalation, groove binding and covalent binding, and they are designed as cations.[3] A positive charge enhances the propensity of a molecule to bind to DNA due to attractive ionic interactions between the cation and the phosphate backbone.[4] Azonia aromatic heterocycles are a representative family of DNA intercalators with good fluorescence properties and some examples have been used as fluorescent probes.[5] Its binding to DNA is characterized by the insertion of planar aromatic rings between the DNA base pairs through π-stacking interactions.[6] While coralyne is probably the most widely studied example of this kind of cation, which contains a quaternary bridgehead nitrogen atom in the core heterocycle,[7] this interest has also led to a significant amount of research on different related compounds that contain a quinolizinium system as the core heterocycle,[8] with recent significant contributions by Ihmels and col.,[9] Becq and col.,[10] and us,[11] *inter alia.*[12]

Less attention has been paid to other azonia heterocycles, despite the fact that some other cationic systems with a quaternary bridgehead nitrogen atom have shown similar characteristics as DNA intercalators.[13] In this sense, we very recently described a dibenzopyridoimidazocinnolinium cation formed by a hexacyclic azonia aromatic system. This compound showed interesting fluorescence properties and DNA-binding ability by intercalation, with a marked preference for AT-rich sequences.[14] Due to its high fluorescence quantum yield (0.32 in 5% DMSO/water and 0.46 in MeOH) and affinity for DNA (binding constant of ~4.5×10^5 M^{-1}), this compound is a promising candidate for the design of fluorescence probes for DNA, although its fluorescence intensity, as in most azonia derivatives,[6,15] is quenched upon complex formation with DNA due to a photoinduced electron-transfer reaction between the excited dibenzopyridoimidazocinnolinium cation and the nucleic bases.

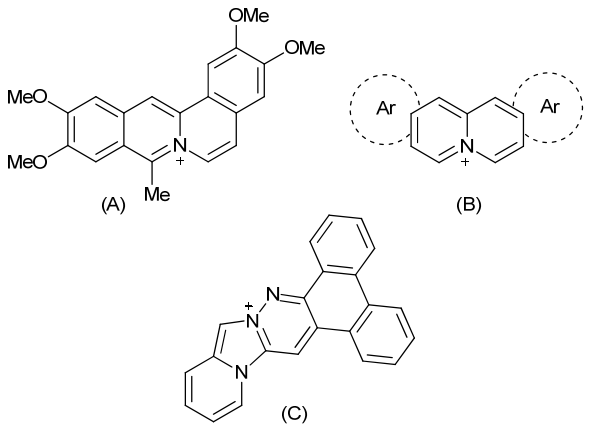

Figure 1. Structure of coralyne (A), general structure of quinolizinium-based azonia cations (B) and the dibenzopyridoimidazocinnolinium cation (C).

[a] *Departamento de Química Orgánica y Química Inorgánica, Instituto de Investigación Química "Andrés M. del Río" (IQAR), Universidad de Alcalá, 28805-Alcalá de Henares, Madrid, Spain.*
[b] *Departamento de Química Analítica, Química Física e Ingeniería Química, Universidad de Alcalá, Spain.*
[c] *Departamento de Biología de Sistemas, Universidad de Alcalá, Spain.*

Electronic Supplementary Information (ESI) available: [details of any supplementary information available should be included here]. See DOI: 10.1039/x0xx00000x

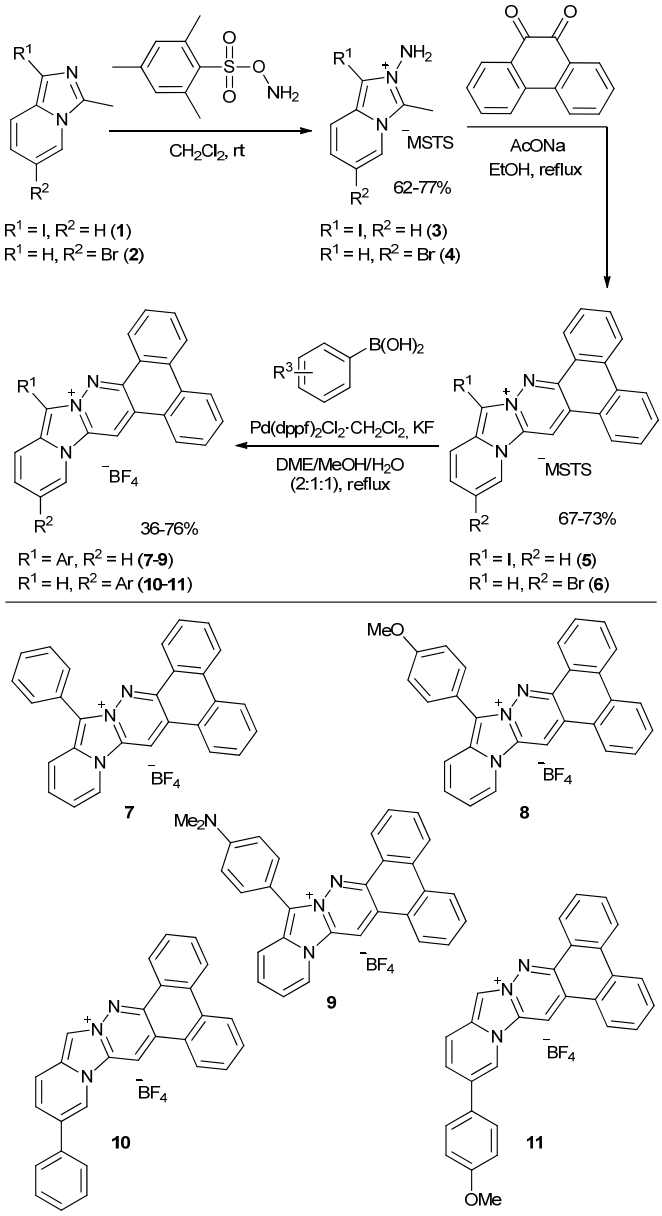

Scheme 1. Synthesis of substituted dibenzopyridoimidazocinnolinium cations.

Taking into account this previous work, we report here the synthesis of four planar dibenzopyridoimidazocinnolinium cationic ligands with appropriate potential DNA-binding properties as intercalators. These free ligands absorb far from the nucleic bases, possess low intrinsic fluorescence and their photophysical properties can be modulated by the incorporation of different aryl donor substituents to the acceptor dibenzopyridoimidazocinnolinium core. In addition to the translational and rotational diffusion of these free ligands in low viscosity solvents, the possible rotation around the substituent–aryl bond could also result in an additional non-radiative deactivation of the excited state of the fluorophores. Both effects should be diminished in the presence of DNA due to the reduction in the molecular and conformational flexibility of the fluorophore:DNA complex, which in turn should lead to a light-up effect.[9f,16]

Moreover, the potential of these compounds for cell staining was investigated in living HeLa cells by confocal microscopy imaging. The results of this analysis showed a remarkable capacity of these azonia cations for active uptake and accumulation by living cells, with complex patterns of intracellular distribution.

Results and discussion

Synthesis of dibenzopyridoimidazocinnolinium cations

Substituted dibenzopyridoimidazocinnolinium cations were readily synthesized in three steps from imidazopyridines **1**, which were obtained in 89% yield from 3-methylimidazo[1,5-*a*]pyridine[17] and *N*-iodosuccinimide, and **2**[18] by a Westphal condensation and a Suzuki cross coupling reaction. In this way, these halolimidazopyridines were aminated with *O*-(mesitylsulfonyl)hydroxylamine (MSH)[19] to give derivatives **3** and **4**, which were subsequently treated with 9,10-phenanthrenequinone and base in a Westphal condensation[20] to afford the dibenzopyridoimidazocinnolinium cations **5** and **6**. Finally, a Suzuki reaction, using the corresponding boronic acid, potassium fluoride and catalytic amounts of the [1,1-bis(diphenylphosphino)ferrocene]-dichloropalladium(II) complex,[21] on these derivatives led the formation of chromophores **7**–**11** in reasonable yields (Scheme 1).

Ligand-DNA binding

Experiments

As an example, the absorption spectra for dilute solutions of ligands **7** and **10** in 5% DMSO/water at 25 °C are shown in Figure 2. Spectra for other cationic ligands in the same solvent and temperature at different concentrations are provided in the supporting information (Figure 1S). The wavelengths of the absorption bands and molar absorptivities at the excitation wavelength (λ_{max}) are listed in Table 1 for the emission spectra along with the locations of emission bands, fluorescence quantum yields (using as the standard, Rhodamine 101 or Coumarin 153 in solution in methanol and ethanol, respectively)[22] and other photophysical parameters.

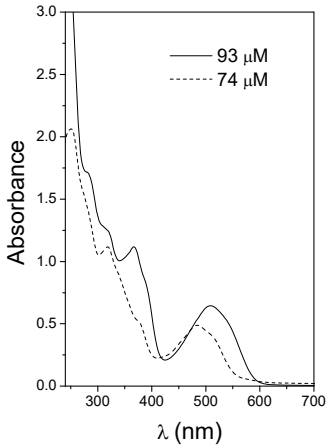

Figure 2. Absorption spectra for dilute solutions of **7** and **10** (dashed line) in 5% DMSO/water (93 and 74 μM respectively) at 25 °C.

A correlation was found between the electron-donating capabilities of the substituents of dibenzopyridoimidazo-cinnolinium cations and the relative position of the maximum of the intramolecular charge transfer (ICT state) low energy absorption bands. The electron-donating capability increased in the order I<C_6H_5<$MeOC_6H_4$<$Me_2NC_6H_4$ and a monotonous bathochromic displacement of ITC absorption bands were observed for ligand **5**, **7**, **8** and **9**. Something similar occurred for **6**, **10** and **11** where the ICT absorption bands were also shifted to longer wavelengths when increasing substituent donating capabilities (Br<C_6H_5<$MeOC_6H_4$).

The emission spectra of dilute solutions of ligands **7** and **10** in 5% DMSO/water (8.27×10^{-6} and 1.16×10^{-5} M) (λ_{exc} of 512 and 488 nm, respectively) are shown in Figure 3 along with the corresponding spectra upon addition of DNA during titration. The spectrum of **7** exhibited a band at ~587 nm whereas the spectrum of **10** displayed a band centred at ~557 nm, which was accompanied by a shoulder at 589 nm. A hypsochromic displacement by ~15 nm of the emission maximum was observed during the titration experiments for **7**. For ligand **10**, however, the peak intensity increased relative to the intensity of the shoulder. In both cases a significant increase in the fluorescence intensity was observed. The emission spectra (depicted in Figure 2S) for other ligands were quite similar to that of **7**, with a single band (as is the cases of **8** and **9**), or that of **10**, which contained emission double bands (**5**, **6** and **11**). In the latter case, the addition of DNA led to changes in the intensity ratio of the two bands. It should be mentioned that the fluorescence emission intensity for all ligands increased to a greater or lesser degree during DNA titration. The exception was **9** whose fluorescence, which was already very low (Table 1), decreased on addition of DNA.

The fluorescence spectra of dilute solutions of free ligands showed analogous trends such as the absorption spectra for the correlation between the electron-donating capabilities of the substituents in both series (**5**, **7**, **8** and **9** or **6**, **10** and **11**) and the location of the emission bands. However, there is an exception; the emission spectrum for **9** exhibits the maximum at 534 nm, which is a rather low wavelength (Table 1, Figure 1S of the SI). This behavior may arise from the dimethylamine group twisting, which affects the stability of the ITC complex (TITC) and therefore the fluorescence features. A consequence of this emission shift is the strong overlapping between both absorption and emission spectra for ligand **9**. The decreasing of the fluorescence upon addition of DNA is most likely related with a radiative reabsorption of the emission.

On the other hand, it is known that fluorescence quantum yields usually decrease with the electron substituent donating nature. The additional non-radiative deactivation excited state path arising from the dimethylamine twisting in the TICT may also contribute to this low fluorescence quantum yield and <τ> decreasing for ligand **9**.[11b,23]

Excitation spectra (Figure 3S of the ESI) recorded at the maximum of emission intensities exhibited features similar to the corresponding absorption spectra and the variation in the intensity on addition of DNA behaved like their corresponding emission spectra.

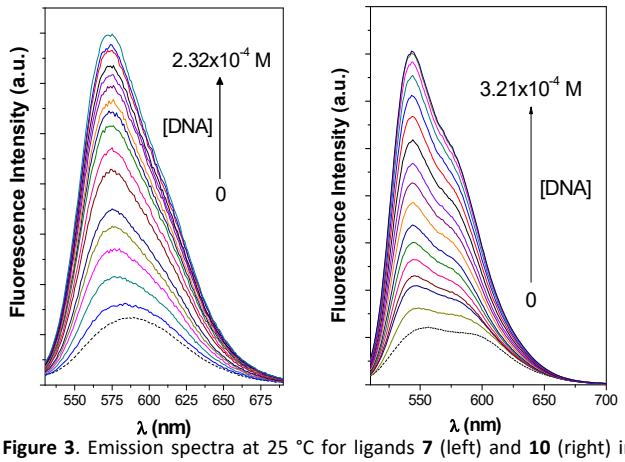

Figure 3. Emission spectra at 25 °C for ligands **7** (left) and **10** (right) in 5% DMSO/water in the free state and upon the addition of DNA aliquots ([**7**] = 8.27×10^{-6} M, [**10**] = 1.16×10^{-5} M).

The normalized variation of the fluorescence intensities of **7** and **10** calculated as $(I - I_0)/I_0$ (I measured as the area under the spectra and subscript zero means in the absence of DNA) versus the [DNA]/ligand molar ratios obtained from the emission and excitation spectra at 25 °C are shown in Figures 4 a and b. Similar representations for other ligands are provided in Figure 4S of the supporting information. The shapes of the curves indicate a binding interaction to a greater or lesser degree for all of the ligands with DNA. The variation of the fluorescence anisotropy (*r*) monitored at the maximum of emission, upon excitation at the wavelength used to collect the fluorescence spectra, versus [DNA] (eq. 10S of ESI) is shown in Figure 4(c). The *r* values for solutions of **7** and **10** at 25 °C in the absence of DNA denote different orientations of the absorption and emission transition moments, molecular sizes and/or rotational diffusion in a low viscosity aqueous medium. The *r* values for both ligands increased with [DNA], which is typical behaviour for the formation of ligand:DNA complexes for which the rotational relaxation times are higher than those of the free ligands. Other cationic ligands, including **9**, exhibited similar increases in *r* upon DNA addition (Figure 5S of ESI).

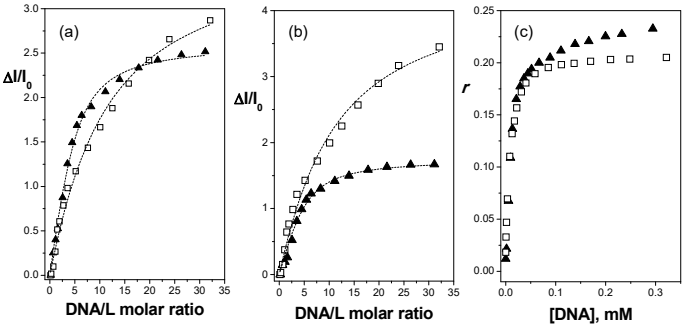

Figure 4. Normalized variation of the fluorescence intensity ($\Delta I/I_0$) obtained from emission spectra (a) and excitation spectra (b) for ligands **7** (▲) and **10** (□)in buffer solutions ([**7**] = 8.27×10^{-6} M, [**10**] = 1.16×10^{-5} M) versus DNA/ligand molar ratios (*R*) during titrations. (c) Fluorescence anisotropy (*r*) changes versus [DNA].

Table 1. Selected photophysical data for ligands in 5% DMSO/water at 25 °C. (p) and (s) denote peak and shoulder, respectively. Fluorescence quantum yields (ϕ_f) were obtained using Rhodamine 101 (*) or Coumarin 153 (**) methanol and ethanol, respectively, as standards.

Compound	I_∞/I_0 (***)	λ_{max} (nm)	ε ($M^{-1}cm^{-1}$) at λ_{max}	$\lambda_{em,\,max}$ (nm)	ϕ_f (at $\lambda_{em,max}$)	$<\tau>$ (ns)	10^{-4} K (M^{-1}) (n)
5	3.60	277(s),318(p),339(s), 358(p),377(s),460(s), **497**(p), 526(s)	8204	548(p)/574(p)	9.8×10^{-3} (*)	3.7	9.6 ± 1.1 (8.5 ± 0.8)
6	1.35	249(p),280(s),305(s), 315(p),345(s),366(s), 441(s), **471**(p),500(s)	9217	533(p)/556(s)	0.03 (**)	2.3	3.7 ± 2.8 (8.6 ± 1.4)
7	2.04	321(s),367(p),387(s), **512**(p),540(s)	6418	587(p)	0.04 (*)	5.4	7.7 ± 2.2 (4.8 ± 0.7)
8	3.62	246(p),285(s),322(s) 372(p),394(s),**532**(p)	5358	621(p)	2.7×10^{-3} (*)	1.2	1.8 ± 0.4 (7.7 ± 1.4)
9	0.33	244(p),302(p), **396**(p),566(p)	1102	534(p)	1.1 10^{-3}(*)	very low	~10^6 n<1
10	3.95	250(p),272(s),318(p), 378(s), **488**(p),515(s)	6970	552(p)/593(s)	0.11 (**)	7.5	0.96 ± 0.1 (3.7 ± 0.2)
11	3.30	246(p),275(s),313(s), 349(s), **497**(p),530(s)	4920	555(s)/604(p)	2.26×10^{-3} (*)	3.4	3.7 ± 0.3 (2.0 ± 0.2)

(***) Measure of the fluorescence intensity enhancement (or decrease), from the I_∞/I_0 ratios.

The curves depicted in Figure 4(a) and Figure 4S(a), which are the result of the adjustment of the experimental data to equation 9S (see ESI), provide values for the association constants *K* and n values collected in Table 1. These values are in the order of 10^4 M^{-1} – as found for some other derivatives of quinolizinium DNA intercalators already reported by us and others.[6,13,14] The average number of nucleic base pairs per bound ligand was in the range ~2–9. Despite the special characteristics of emission, whose fluorescence decreases in the presence of DNA, the analysis for ligand **9** was also performed. Results show an atypical association constant that was two orders of magnitude higher than that of other ligands and a surprisingly small (below 1) n value. These data could denote strong DNA–**9** interactions and, consequently, this system would not fulfill the requirements for the application of Equation 9S. However, it is also true that reabsorption of the emission could make the analysis of titration data for **9** somewhat uncertain. The decreasing of the fluorescence intensity during its DNA titration is also likely to be related to this effect, as stated before.

As a measure of the ligand fluorescence enhancement (or diminution for ligand **9**) upon DNA complexation, the fluorescence intensity (I_∞/I_0) ratios obtained from the experimental data adjustments to equation 9S are listed in Table 1. The curves in Figure 4(b) (and Figure 4S(b) of ESI) reproduce the adjustment to equation 9S for the experimental data obtained from the excitation spectra by using *K* and n values that were previously calculated from emission spectra.

Fluorescence intensity decay profiles obtained at 25 °C for dilute solutions of free ligands 7 and 10 in 5%DMSO/water were fitted to double exponential decays to give weighted average lifetimes ($<\tau>$) of 5.4 ns and 7.5 ns, respectively (eq. 11S of ESI). The presence of DNA made the decay intensity profiles more complex (the sum of three exponential decays) but there was no apparent monotonic variation in $<\tau>$ with the DNA/L molar ratios. In fact, the average $<\tau>$ values observed for both ligands in the presence of DNA were 5.5±0.2 and 7.2±0.8 for measurements performed in the 0–4 and 0–8 range of DNA/L molar ratios, respectively.

The circular dichroism (CD) spectrum in the region of the DNA absorption for the free ctDNA (Figure 5) shows the typical B-form spectrum with bands of opposite sign centred at ~278 nm (+) and ~245 nm (–) due to base stacking and right-handed polynucleotide helicity, respectively.[24] According to some authors, groove binding and the electrostatic interactions between small molecules and DNA show hardly any perturbations in these two bands, but intercalation due to strong base stacking interactions and stable DNA conformations usually enhances the intensity of both bands.[25] However, several other authors assert that intercalation interrupts interactions between bases, thus weakening stacking and consequently decreasing the intensity of both bands.[26] As depicted in Figure 5, the intensity of the high-energy negative band (at 245 nm) decreased upon increasing the concentration of ligands **7** or **10** (or L/DNA ratio). However, an increase in the intensity of the positive band (at 278 nm) was observed for all of the cationic ligands studied. As occurred for the intercalation of other compounds, these ligands absorbed below 300 nm where the low energy DNA band is also located. Consequently, the ICD spectra of the complexed ligand overlapped the 278 nm DNA band, thus modifying the expected intensity trend with L/DNA ratio.[14]

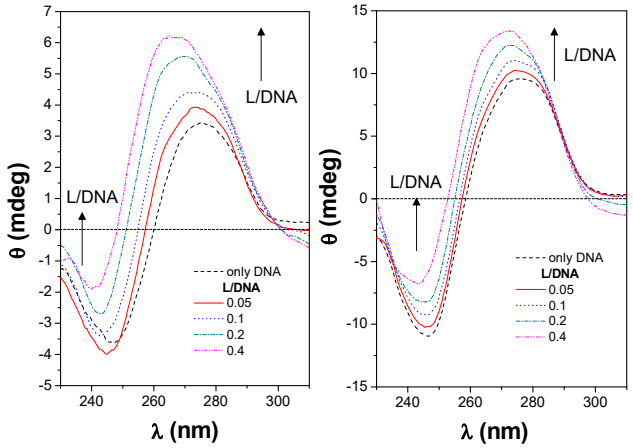

Figure 5. CD spectra (ellipticity, θ) in the region of DNA absorption for **7** (left) and **10** (right) in 5% DMSO/water solutions in the presence of DNA ([DNA] = 7.20×10^{-4} M and 6.70×10^{-4} M, respectively) at several ligand/DNA molar ratios. Measured at 25 °C (0.1 cm path cuvette).

The observation in Figure 6 of a CD signal in the region where achiral cationic ligands predominantly absorb is a consequence of the formation of ligand complexes with DNA. An intercalator exhibits a negative (positive) ICD when the transition moment for the corresponding absorption band is oriented parallel (perpendicular) to the base pair pocket axis or perpendicular (parallel) to the pseudo-dyad axis. The ICD spectra of a groove-bound ligand usually exhibit a more intense positive signal than an intercalated ligand.[6,24a-b,27]

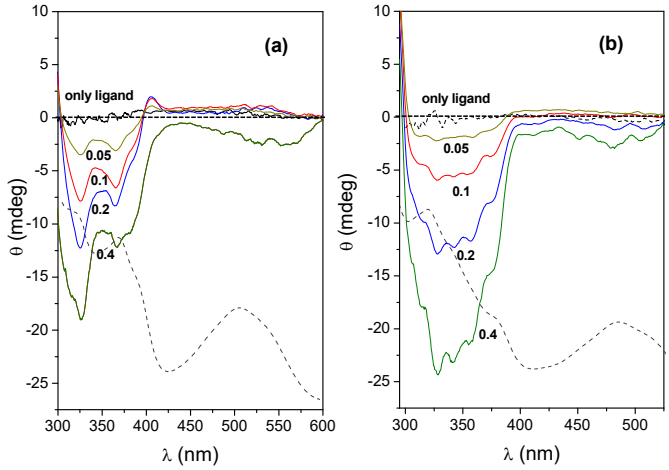

Figure 6. Ellipticity (θ) measured at 25 °C for ligands (a) **7** and (b) **10** in 5% DMSO/water solutions in the presence of DNA ([DNA] = 1.95×10^{-4} M and 3.0×10^{-4} M, respectively) at several ligand/DNA molar ratios. Superimposed are the absorption spectra for both ligands (---, grey) (1 cm path cuvette).

The ICD spectra of free cationic ligands **7** and **10** are shown in Figure 6 along with those for the ligands in the presence of DNA at different L/DNA molar ratios with constant [DNA]. No CD signal was observed for isolated achiral ligand **7** and **10** solution, as expected. CD spectra of DNA solutions in the presence of ligands at any of the ratios used exhibit, albeit relatively weak, Cotton effects whose intensities depend on the L/DNA ratios. Both spectra denote the absence of exciton coupling, thus ruling out any potential ligand aggregation at the concentrations used.[6,27c] The ICD spectra in Figure 6S of the supporting information show molar ellipticities ([θ]), which remove the influence of ligand concentration and the optical path. The ICD spectra depicted in Figure 6 and Figure 6S of the ESI contain two regions that correspond to distinguishable bands in the absorption spectra: (i) a relatively intense negative band extending below the ~410 nm band; and (ii) a much weaker band that covers wavelengths above ~410 nm and whose signal was near zero or slightly positive. The latter visualization is clearer in the molar ellipticity spectra in Figure 6S of the ESI. Assuming that the transition moment of the band that appeared at lower wavelengths was almost perpendicular to the long ligand axis, the band observed at lower energies would correspond to the transition moment that is oriented almost parallel to the long axis. The negative sign of the ICD high energy band observed in both ICD spectra is consistent with an intercalation of the ligand with its short-molecular axis parallel to the DNA binding pocket.[6,24a-b,27d] However, the near absence or slight positive sign of the ICD signal for the low energy band is consistent with a transition moment oriented close to 45° (or slightly >45°) to the base pair binding pocket. The absence of large positive ellipticities also rules out the presence of ligand-DNA groove binding interactions.

Molecular Mechanics and Molecular Dynamics

Protocols on the binding of intercalators to DNA are described in the ESI. The total binding energies, along with the van der Waals and electrostatic contributions, for the intercalation of ligands **7** and **10** with the DNA fragment between the central AT, TA pair of bases as a function of the *oo'* distance along the *y* coordinate are depicted in Figures 8S and 9S in the ESI. This intercalation of ligands took place by the major groove with the long axis parallel (Figure 8S) or perpendicular (Figure 9S) to the base pair pocket. Intercalation occurred without significant potential barriers when the ligand approached with its main long axis parallel to the base pair pocket (Figure 8S). However, the barriers observed at positive *y* coordinates for a perpendicular approach (Figure 9S) indicated that ligands with this orientation would prefer to approach by the minor groove (apparently without any barriers). In both cases, electrostatics interactions were mainly responsible for the stabilization. Minimum binding energy (MBE) structures for both complexes with DNA are depicted in the same Figures. The orientation of the ligands relative to the base pair pocket axis barely changed from the initial one during approach.

The left-hand panels in Figure 7 (and Figure 10S of ESI) show the histories of the **7**/DNA and **10**/DNA binding energies and contributions obtained from an analysis of the 1.0 ns MD trajectories at 300 K on the four water-solvated MBE structures (represented in Figure 8S Figure 9S of the ESI). The results reveal that ligand-DNA interactions are favourable throughout the whole trajectory for all of the intercalations. As with MM, the most important contributions to stabilization are the electrostatics. The van der Waals interactions contribute barely 10% of the total binding energy. The averages of several energetic and geometrical parameters obtained in the analysis

of the MD trajectories are listed in Table 1 of the supporting information.

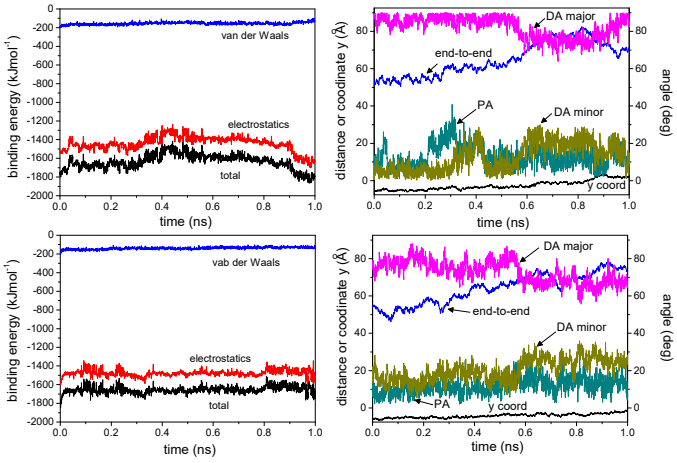

Figure 7. (Left panels) Histories of binding energies, electrostatics and van der Waals contributions; (right panels) histories for the *y* coordinate (y coord) of the centre of ligands, for the end-to-end twelve nucleotide DNA fragment distance (end-to-end), for the averaged angles between the plane of both AT and TA pairs of bases and the plane of ligand rings (PA) and the angles between the pocket bases axis and the long (DA major) or the short ligand axis (DA minor) obtained from the analysis of the 1 ns MD trajectory at 300 K starting from the minimized MBE structure of the **7**/DNA complex (upper panels) and **10**/DNA (bottom panels) by approaching the ligand with its long axis perpendicular to the base pair pocket.

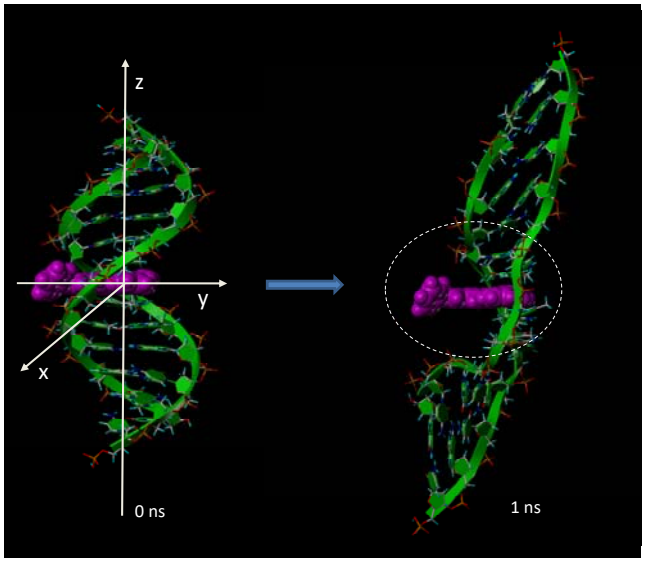

Figure 8. Snapshots of the 1 ns MD trajectory at 300 K for the **10**/DNA complex. The figure shows the location of ligand **10** at time = 0 ns (minimized MBE structure where the long ligand axis is oriented perpendicular to the base pair pocket axis) and at time = 1 ns from the beginning of the trajectory (right).

The histories of the y coordinate at the centre of ligands **7** and **10** are depicted in the right-hand panels of Figure 7 (Figure 10S of ESI) for both **7**/DNA and **10**/DNA complexes for the ligand approaching DNA with its long axis perpendicular (parallel) to the base pair pocket. The intercalators tend to stay close to a y coordinate of zero, slightly outside the major or minor groove faces. The averages of these coordinates throughout the MD trajectories were −2.5±2.5 and −4.2±1.1 Å (+0.1±3.0 and −1.1±1.8 Å) for **7**/DNA and **10**/DNA complexes by perpendicular (parallel) ligand approach, respectively. It can be seen from Figure 7 (Figure 10S of ESI) that the 1 ns MD did not substantially change the initial orientation of the ligand relative to the pocket bases axis. The average during the whole 1 ns trajectories of the angles between the long (short) ligand axis and the base pair pocket axis for both types of approach are provided in Table 1S (ESI). For example, for the perpendicular ligand-to-DNA base pair pocket axis approach, the average values for the angle of the short (long) axis and the base pair pocket axis were 12.6±7.4 and 20.4±5.8° (82.2±5.8° and 72.9±5.9°) for the **7**/DNA and **10**/DNA complexes, respectively. These results are reasonably consistent with a negative high-energy band (at $\lambda \leq 410$ nm) whose transition moment is oriented along the short axis of the ligand, which in turn is nearly parallel to the base pair pocket axis. The almost zero or positive low energy band at $\lambda \geq 410$ nm is consistent with an angle between the long ligand axis and the base pair pocket axis of 45° or larger. The structures for **7**/DNA and **10**/DNA complexes when ligands approached the DNA pocket perpendicularly at the beginning, during or at the end of MD trajectory nearly agreed with the sign observed in the ICD spectra.

As an example, the minimized MBE starting structure (at time = 0 ns) and at the end of the trajectory for the **10**/DNA complex are shown in Figure 8. For the latter structure, **10** was oriented with its short axis nearly parallel to the pocket axis with the phenanthrene group lying inside this pocket and most of the structure slightly outside by the minor groove face. In addition, as one would expect for ligands that intercalate, the angle between the AT and TA base pair planes and the plane of both ligands were close to zero. In fact, averages of 11.2±6.5° (13.2±5.9°) and 12.9±7.9° (11.9±4.3°) for **7**/DNA and **10**/DNA systems and parallel (perpendicular) orientation, respectively, were obtained (Table 1S of ESI). Another characteristic upon intercalation is the slight unwinding of the DNA double helix, which becomes distorted and lengthened upon intercalation. From the initial DNA fragment, intercalation caused the end-to-end DNA helix distance to increase significantly with time for all of the complexes (Figure 7 and 10S). The averages of these distances are collected in Table S1.

Live-cell studies

The toxicity of compounds **5**, **6**, **10** and **11** on living cells in culture was determined by the standard MTT assay using the HeLa cell line after 24 hours of exposure to the compounds. The estimated apparent lethal dose 50% (LD_{50}) is 2.2×10^{-4} M for compounds **6** and **11**, 1.5×10^{-5} M for **5** and 2.3×10^{-5} M for **10**.

The capacity of compounds **5**–**11** for live-cell staining, uptake and intracellular distribution was studied by confocal fluorescence microscopy imaging using HeLa cells grown on coverslip-bottom dishes in Dulbecco's Modified Eagle's Medium supplemented with 10% foetal bovine serum (DMEM,

10% FBS). This study was aimed to detect possible compounds with application in cell biology and microscopy, as fluorescent dyes for living cells or specific probes for subcellular organelles or structures. In addition, we can take advantage of the fluorescent properties of the compounds to directly visualize their internalization and distribution in living cells, which may be a valuable information to follow possible pharmacological applications. The results are summarized in Figure 9. The analysis showed a marked capacity of all compounds for live-cell staining of intracellular structures. The results suggest an asynchronous, apparently active uptake by some endocytic mechanism rather than by passive diffusion through the plasma membrane. Each compound showed a very distinct pattern of intracellular distribution, which suggests some sort of specific intracellular trafficking or recognition by different cellular components. In all these cases, the overall pattern of fluorescence suggests that these compounds are mostly confined to membranous vesicles and organelles and that they do not diffuse freely in the cytoplasm or nucleoplasm.

The compounds also show very diverse spectral properties inside the living cells, including fluorescence in different colours from the same compound associated with certain areas in particular subcellular structures. The variation in the spectral properties may be due to the different conditions in specific subcellular environments, to the association with particular proteins or other cellular components, or even some intracellular or organelle-localised metabolic modification of the compounds. The apparent exclusion, or faint fluorescence emission, from the nucleus in several studied dibenzopyridoimidazocinnolinium derivatives (**5**, **6**, **8**, **9** and **11**) is remarkable. Compounds **5**, **8**, **9** and **11** show fluorescence in a single excitation-emission channel, whereas compounds **6**, **7** and **10** exhibit a more complex pattern with non-overlapping fluorescence in two (**7**, **10**) or even three (**6**) different excitation-emission channels.

The results obtained for single-channel emitting compounds are summarized in the upper row of Figure 9. Compound **5** (green emission channel) showed brightly fluorescent, discrete vesicle-like structures in the cytoplasm, and a slightly diffuse and non-homogeneous fluorescence inside the nucleus. Compound **8** (red emission channel) showed brightly fluorescent reticular structures in the cytoplasm and a very weak, and non-homogeneous fluorescence inside the nucleus. Compound **9** (infrared emission channel, shown in pseudocolour in Figure 9) showed granular disperse fluorescence in the cytoplasm and some very faintly fluorescent structures inside the nucleus. Compound **11** (red emission channel) showed brightly fluorescent, discrete vesicle-like structures in the cytoplasm and a very weak fluorescence inside the nucleus, with a distribution similar to that of compound **8**.

As indicated above, compounds **6**, **7** and **10** show fluorescence in two or more channels. These results are summarized in the lower row of Figure 9 (panels a, b and c). Compound **6** showed a strong red emission (a) from brightly fluorescent, abundant and well delineated vesicle-like structures located in the cytoplasm, as well as a more disperse or diffuse, partially overlapping green (b) and blue (b) emission from the cytoplasm. The nucleus showed weak fluorescence in the three channels, which was more diffuse and possibly overlapping in the case of green and blue, and a few relatively bright points in the red channel. Compound **7** showed intense emission from brightly fluorescent structures located in the cytoplasm, possibly endoplasmic reticulum (ER), both in the red (a) and green (b) channels and partially co-localizing (yellow in overlay, c). The nucleus showed a diffuse fluorescence in the red channel (a), but in the green channel (b) it exhibited a complex staining pattern with a well delineated nuclear envelope and non-homogeneous reticular or granular staining in the nucleoplasm. Compound **10** showed a very strong emission in the red channel (a) from brightly fluorescent structures located in the cytoplasm, possibly mitochondria, and also a weaker, diffuse emission form the nucleoplasm. In the green channel (b), this compound showed an intense staining of the nucleus, with a complex pattern similar to that of compound **7**. The red and green emissions clearly did not overlap, as shown in the overlay image (c).

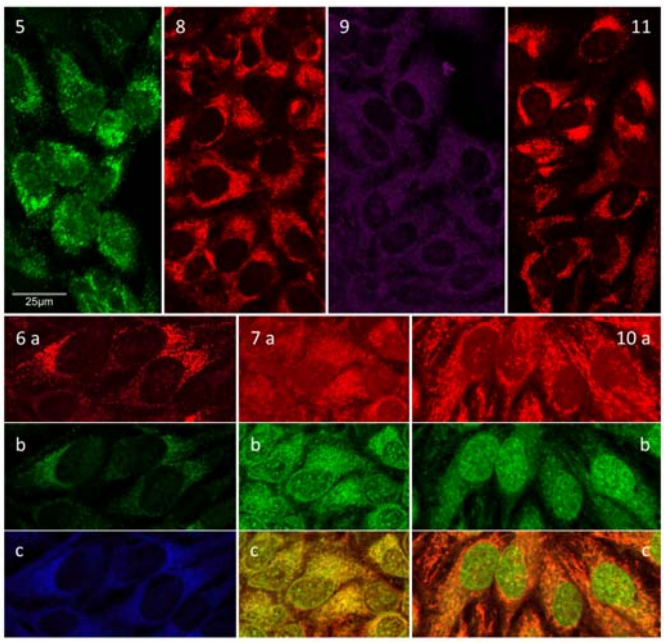

Figure 9. Confocal fluorescence microscopy of living HeLa cells in culture after 1 hour of exposure to the indicated compounds **5** to **11**, 50 mM in DMSO, diluted 1:400 in culture medium (125 uM final). Scale bar 25 µm common for all panels. Top row: compounds **5**, **8**, **9** and **11** showing fluorescence in a single channel. Bottom row: compounds **6**, **7** and **10** showing fluorescence in two or more channels. Control cells not exposed to compound were not fluorescent under the same conditions (not shown).

Spectral shifts of single fluorescent dyes depending on different intracellular microenvironments are not uncommon.[28] As previously mentioned, the most likely origin of this phenomenon is the great diversity of localised microenvironments inside a living cells, few of which are really known and even less of them can be readily identified by morphological characteristics in a microscopy image. Preliminary experiments were carried out trying to mimic *in*

vitro some of the most common and known organelle conditions, such as acidic (lysosomes and other ER-derived vesicles) or basic pH and reducing environment (mitochondria). Even the possibility of some metabolic transformation was investigated by spectroscopic analysis of compound **10** recovered from the stained cells. The results (not shown) did not reproduce in any case the spectral variations observed *in vivo*. The intracellular microenvironments are far more complex and diverse than the explored conditions and many other aspects may be involved. The compounds become highly concentrated in small subcellular compartments, very likely by some active and specific processes, and may be also complexed with other also localised molecules. Some of these conditions are almost impossible to reproduce *in vitro*. Additionally, confocal microscopy uses intense laser light for excitation and extremely sensitive detectors to register the fluorescence emission, and sets of filters that give rise to discrete monochrome images. The apparently dramatic spectral shifts may well arise from minor changes slightly affecting just a tail of a spectral excitation or emission band. In any case, the live cell staining capacity, with almost no background fluorescence in wash-free conditions observed in these compounds, and the complex pattern exhibited by **6**, **7** and **10**, make them very promising tools with potential applications in biological research, cell biology and confocal microscopy imaging.

Experimental

Synthetic procedures

General information. All chemicals were reagent grade, purchased of the highest commercial quality from Sigma-Aldrich or Acros Organics and used without further purification, unless stated otherwise. Reactions were monitored by thin-layer chromatography (TLC) carried out on 0.25 mm E. Merck silica gel plates (60FS-254) using UV light to visualize the compounds. Column chromatography was performed using silica gel (60 F254, 70–200 mm) as the stationary phase. All melting points were determined in open capillary tubes on a Stuart Scientific SMP3 melting point apparatus and are uncorrected. IR spectra were obtained on a Perkin-Elmer FTIR spectrum 2000 spectrophotometer. ^{1}H and ^{13}C NMR spectra were recorded with either Varian Mercury VX-300, Varian Unity 300 or 500 MHz spectrometers at room temperature. Chemical shifts are given in ppm (δ) downfield from TMS. Coupling constants (J) are in Hertz (Hz) and signals are described as follows: s, singlet; d, doublet; t, triplet; br, broad; m, multiplet; ap, apparent etc. High-resolution analysis (TOF) was performed on an Agilent 6210 time-of-flight LC/MS. 3-Methylimidazo[1,5-*a*]pyridine,[17] imidazopyridine **2**,[18] and *O*-mesytilenesulfonylhydroxylamine (MSH)[19] were prepared following the procedures described in the literature.

1-Iodo-3-methylimidazo[1,5-*a*]pyridine (1). *N*-Iodosuccinimide (225 mg, 1.00 mmol) was added to a solution of methylimidazo[1,5-*a*]pyridine (124 mg, 0.94 mmol) in a mixture of anhydrous CH_2Cl_2 (8 mL) and anhydrous DMF (4 mL). After stirring for 1.5 hours at room temperature the reaction was stopped by addition of water and was extracted with CH_2Cl_2. The organic layer was washed with brine and saturated aqueous $Na_2S_2O_3$. The organic layer was dried with Na_2SO_4. No further purification was needed. The desired compound was obtained in 89% yield (216 mg). M.p: 65–67 °C. IR (KBr) ν cm^{-1}: 2921, 1648, 1630, 1083, 744. ^{1}H NMR (300 MHz, $CDCl_3$) δ 7.51 (dtap, *J* = 7.1, 1.2 Hz, 1H), 7.10 (dtap, *J* = 9.2, 1.3 Hz, 1H), 6.59 (ddd, *J* = 9.2, 6.4, 1.0 Hz, 1H), 6.54–6.41 (m, 1H), 2.52 (s, 3H). ^{13}C NMR (75 MHz, $CDCl_3$) δ 136.8, 131.9, 120.8, 118.9, 118.1, 112.9, 70.2, 12.4. HRMS (ESI-TOF) for $C_8H_7IN_2$ m/z (Calc.): 258.9712 m/z (found) 258.9710.

General procedure for the *N*-amination of heterocycles. A solution of MSH (0.75 mmol, 1.5 equiv) in dry CH_2Cl_2 (3 mL) was added dropwise to a solution of the starting heterocycle (0.50 mmol, 1 equiv) in dry CH_2Cl_2 (3 mL). The reaction mixture was stirred at room temperature for between 5 and 24 hours. After the appropriate time the reaction mixture was filtered, the solid phase was isolated and washed with CH_2Cl_2 and petroleum ether to give the desired product.

2-Amino-1-iodo-3-methylimidazo[1,5-*a*]pyridin-2-ium 2,4,6-trimethylbenzenesulfonate (3). Following the general procedure for the *N*-amination of heterocycles a solution of MSH (1212 mg, 5.63 mmol) in CH_2Cl_2 (8 mL) was added dropwise to a solution of **1** (969 mg, 3.75 mmol) in CH_2Cl_2 (8 mL). The reaction mixture was stirred for 24 hours. After this time the product was isolated to obtain the desired product in 62% yield (1110 mg). M.p: 210–212 °C. IR (KBr) ν cm^{-1}: 3273, 1206, 1193, 1083, 1015, 674. ^{1}H NMR (300 MHz, DMSO d_6) δ 8.40 (d, *J* = 7.3 Hz, 1H), 7.52 (d, *J* = 9.2 Hz, 1H), 7.26–7.09 (m, 2H), 6.89 (s, 2H), 6.70 (s, 2H), 2.89 (s, 3H), 2.46 (s, 6H), 2.14 (s, 3H). ^{13}C NMR (75 MHz, DMSO d_6) δ 142.3, 137.1, 135.7, 135.3, 129.3, 124.4, 123.7, 117.7, 116.4, 73.4, 22.3 (2C), 19.8, 9.3. HRMS (ESI-TOF) for $C_8H_9IN_3^+$ m/z (Calc.): 273.9836, m/z (Found): 273.9814.

2-Amino-6-bromo-3-methylimidazo[1,5-a]pyridin-2-ium 2,4,6-trimethylbenzenesulfonate (4). Following the general procedure for the *N*-amination of heterocycles a solution of MSH (237 mg, 1.10 mmol) in CH_2Cl_2 (3 mL) was added dropwise to a solution of **2** (155 mg, 0.73 mmol) in CH_2Cl_2 (3 mL). The reaction mixture was stirred for 7 hours. After this time the product was isolated to give the desired product in 77% yield (238 mg). M.p: 177–180 °C. IR (KBr) ν cm^{-1}: 3485, 3244, 3151, 1656, 1167, 1083, 862, 679. ^{1}H NMR (300 MHz, DMSO d_6) δ 8.82 (dd, *J* = 2.4, 1.1 Hz 1H), 8.09 (d, *J* = 0.7 Hz 1H), 7.72 (dd, *J* = 9.8, 1.1 Hz, 1H), 7.31 (dd, *J* = 9.8, 1.5 Hz, 1H), 7.25 (s, 2H), 6.72 (s, 2H), 2.79 (s, 3H), 2.47 (s, 6H), 2.15 (s, 3H). ^{13}C NMR (126 MHz, DMSO d_6) δ 142.3, 135.7, 135.3, 133.4, 129.3, 126.5, 124.4, 122.5, 118.6, 113.2, 110.5, 22.3 (2C), 19.8, 8.1. HRMS (ESI-TOF) for $C_8H_9BrN_3^+$ m/z (Calc.): 225.9981, m/z (Found): 225.9980.

General procedure for the Westphal condensation. 9,10-phenanthrenequinone (0.72 mmol 1.2 equiv) and sodium

acetate (0.72 mmol, 1.2 equiv) were added to a suspension of the cycloimmonium salt (0.6 mmol, 1 equiv) in EtOH (6 mL). The reaction mixture was stirred and heated under reflux for between 24 and 48 hours. After this time the reaction mixture was cooled down to room temperature. Removal of solvent *in vacuo* gave a residue that was triturated with cold water and filtered. The residue was washed with cold water and AcOEt several times to give a solid that was dissolved in the minimum amount of MeOH. The solution was cooled (ice bath) and cold Et_2O was added until the product precipitated. The solid was filtered off to give the desired compound.

11-Iododibenzo[*f*,*h*]pyrido[1',2':3,4]imidazo[1,2-*b*]cinnolin-10-ium 2,4,6-trimethylbenzenesulfonate (5). Following the general procedure for the Westphal condensation, 9,10-phenanthrenequinone (157 mg, 0.76 mmol) and sodium acetate (62 mg, 0.76 mmol) were added to a suspension of **3** (300 mg, 0.63 mmol) in EtOH (9 mL). The reaction mixture was stirred and heated under reflux for 24 hours. After this time the product was isolated in 67% yield (272 mg). M.p: 204–205 °C. IR (KBr) ν cm^{-1}: 3435, 1642, 1516, 1492, 1379, 1212, 1182, 1013, 760, 676. ^{1}H NMR (500 MHz, DMSO d_6) δ 10.54 (s, 1H), 9.58 (d, *J* = 6.9 Hz, 1H), 9.07 (dd, *J* = 8.1, 1.5 Hz, 1H), 8.87–8.85 (m, 1H), 8.78–8.75 (m, 2H), 8.12 (d, *J* = 9.2 Hz, 1H), 7.97–7.79 (m, 5H), 7.65 (t, *J* = 6.9 Hz, 1H), 6.70 (s, 2H), 2.46 (s, 6H), 2.14 (s, 3H). ^{13}C NMR (75 MHz, DMSO d_6) δ 146.2, 142.3, 135.6, 135.3, 134.9, 132.0, 131.8, 131.3, 130.6, 130.1, 129.3, 129.1, 128.5, 125.9, 125.4, 124.7, 124.3, 123.9, 123.6, 121.8, 117.4, 116.4, 113.7, 67.7, 22.2 (2C), 19.8. HRMS (ESI-TOF) for $C_{22}H_{13}IN_3^+$ m/z (Calc.): 446.0149, m/z (Found): 446.0114.

14-Bromodibenzo[*f*,*h*]pyrido[1',2':3,4]imidazo[1,2-*b*]cinnolin-10-ium 2,4,6-trimethylbenzenesulfonate (6). Following the general procedure for the Westphal condensation, 9,10-phenanthrenequinone (23 mg, 0.11 mmol) and sodium acetate (9 mg, 0.1 mmol) were added to a suspension of **4** (40 mg, 0.09 mmol) in EtOH (3 mL). The reaction mixture was stirred and heated under reflux for 48 hours. After this time the product was isolated in 73% yield (41 mg). M.p: 264–266 °C. IR (KBr) ν cm^{-1}: 3441, 3040, 1645, 1514, 1492, 1384, 1084, 1014, 761, 677. ^{1}H NMR (300 MHz, DMSO d_6) δ 10.55 (s, 1H), 9.90 (s, 1H), 9.40 (s, 1H), 9.01 (d, *J* = 7.3 Hz, 1H), 8.78–8.76 (m, 2H), 8.18 (d, *J* = 9.4 Hz, 1H), 7.99–7.79 (m, 5H), 6.69 (s, 2H), 2.45 (s, 6H), 2.13 (s, 3H). ^{13}C NMR (75 MHz, DMSO d_6) δ 146.7, 135.6, 135.3, 132.6, 132.1, 131.9, 130.8, 130.1, 129.2, 128.6, 128.5, 127.7, 125.3, 124.8, 124.7, 124.5, 124.4, 123.9, 123.6, 122.4, 118.5, 114.0, 110.0, 109.5, 22.2 (2C), 19.8. HRMS (ESI-TOF) for $C_{22}H_{13}BrN_3^+$ m/z (Calc.): 400.0287, m/z (Found): 400.0289.

General procedure for the Suzuki cross coupling reaction. A suspension of compound **5** or **6** (0.12 mmol, 1 equiv), boronic acid (0.24 mmol, 2 equiv), potassium fluoride (0.48 mmol, 4 equiv) and [1,1'-bis(diphenylphosphino)-ferrocene]dichloropalladium(II) complex with dichloromethane (1:1) (0.007 mmol 0.06 equiv) in a mixture of DME, MeOH and water (2:1:1) (4 mL) was stirred and heated under reflux for between 24 and 36 hours. After this time the reaction mixture was cooled to room temperature and MeOH was added. The mixture was filtered and washed with MeOH. The filtrate was concentrated in vacuo to approximately ¼ of its original volume. The mixture was poured into saturated aqueous $NaBF_4$ to change the counter ion. The mixture was stirred for 4 hours and after this time the mixture was filtered to obtain a solid residue. Flash column chromatography (98:2→95:5 CH_2Cl_2/MeOH) on silica was performed on this residue to obtain the desired compound.

11-Phenyldibenzo[*f*,*h*]pyrido[1',2':3,4]imidazo[1,2-*b*]cinnolin-10-ium tetrafluoroborate (7). Following the general procedure for the Suzuki coupling reaction, starting from compound **5** (100 mg, 0.15 mmol), phenylboronic acid (38 mg, 0.30 mmol), potassium fluoride (36 mg, 0.62 mmol) and [1,1'-bis(diphenylphosphino)-ferrocene]dichloropalladium(II) complex with dichloromethane (1:1) (8 mg, 0.009 mmol), and after purification by flash column chromatography (92:8 CH_2Cl_2/MeOH), the desired product **7** was obtained in 36% yield (27 mg). M.p: 275–277 °C (decomposition). IR (KBr) ν cm^{-1}: 3433, 1646, 1528, 1490, 1383, 1059, 767, 703. ^{1}H NMR (500 MHz, DMSO d_6) δ 10.73 (s, 1H), 9.70 (d, *J* = 7.4 Hz, 1H), 8.95 (d, *J* = 8.6 Hz, 1H), 8.90 (d, *J* = 8.1 Hz, 1H), 8.83–8.80 (m, 2H), 8.35 (d, *J* = 9.3 Hz, 1H), 8.20 (d, *J* = 7.4 Hz, 2H), 8.00–7.65 (m, 9H). ^{13}C NMR (75 MHz, DMSO d_6) δ 145.8, 131.9, 131.7, 131.0, 130.5, 129.7, 129.5, 129.0, 128.7, 128.5, 127.3, 125.2, 125.1, 124.8, 124.5, 124.2, 124.1, 123.8, 123.4, 121.5, 118.0, 117.0, 116.6, 113.7. HRMS (ESI-TOF) for $C_{28}H_{18}N_3^+$ m/z (Calc.): 396.1484, m/z (Found): 396.1484.

11-(4-Methoxyphenyl)dibenzo[*f*,*h*]pyrido[1',2':3,4]imidazo[1,2-*b*]cinnolin-10-ium tetrafluoroborate (8). Following the general procedure for the Suzuki coupling reaction, starting from compound **5** (140 mg, 0.22 mmol), *p*-methoxyphenylboronic acid (67 mg, 0.44 mmol), potassium fluoride (51 mg, 0.88 mmol) and [1,1'-bis(diphenylphosphino)-ferrocene]dichloropalladium(II) complex with dichloromethane (1:1) (11 mg, 0.013 mmol), and after purification by flash column chromatography (95:5 CH_2Cl_2/MeOH), the desired product **8** was obtained in 59% yield (67 mg). M.p: 291–292 °C (decomposition). IR (KBr) ν cm^{-1}: 3434, 1644, 1610, 1510, 1382, 1263, 1058, 835, 769, 756. ^{1}H NMR (500 MHz, DMSO d_6) δ 10.54 (s, 1H), 9.59 (s, 1H), 8.76 (m, 4H), 8.30 (d, *J* = 9.2 Hz, 1H), 8.11 (d, *J* = 8.7 Hz, 2H), 7.99–7.62 (m, 6H), 7.37 (d, *J* = 8.8 Hz, 2H), 3.98 (s, 3H). ^{13}C NMR (126 MHz, DMSO d_6) δ 160.0, 152.4, 145.9, 131.8, 130.5, 130.4, 130.3, 129.0, 128.5, 128.4, 127.1, 125.4, 125.0, 124.9, 124.4, 124.2, 123.8, 123.4, 121.2, 118.2, 117.0, 116.4, 116.0, 114.4, 113.6, 55.1. HRMS (ESI-TOF) for $C_{29}H_{20}N_3O^+$ m/z (Calc.): 426.1576, m/z (Found): 426.1577.

11-(4-(Dimethylamino)phenyl)dibenzo[*f*,*h*]pyrido[1',2':3,4]imidazo[1,2-*b*]cinnolin-10-ium tetrafluoroborate (9). Following the general procedure for the Suzuki coupling reaction, starting from compound **5** (124 mg, 0.20 mmol), *p*-dimethylaminophenylboronic acid (66 mg, 0.40 mmol), potassium fluoride (47 mg, 0.80 mmol) and [1,1'-

bis(diphenylphosphino)-ferrocene]dichloropalladium(II) complex with dichloromethane (1:1) (9 mg, 0,01 mmol), and after purification by flash column chromatography (95:5 CH_2Cl_2/MeOH), the desired product **9** was obtained in 41% yield (44 mg). M.p: 260–261 °C (decomposition). IR (KBr) ν cm^{-1}: 3064, 1565, 1409, 1377, 1251, 1216, 1181, 1033, 764, 743. ^{1}H NMR (500 MHz, DMSO d_6) δ 10.59 (s, 1H), 9.60 (s, 1H), 8.90 (d, 2H), 8.78, (d, 2H), 8.28, (d, 1H), 8.02, (d, 2H), 7.92–7.79 (m, 4H), 7.66 (tap, 2H), 7.09 (d, 2H), 3.12 (s, 6H). ^{13}C NMR (126 MHz, DMSO d_6) δ 151.1, 146.4, 132.4, 132.3, 130.0, 129.5, 129.1, 128.9, 127.4, 125.6, 125.5, 124.9, 124.8, 124.4, 124.0, 119.8, 117.8, 116.7, 112.1, 110.9, 100.6. HRMS (ESI-TOF) for $C_{30}H_{23}N_4^+$ m/z (Calc.): 439.1917, m/z (Found): 439.1915.

14-Phenyldibenzo[*f*,*h*]pyrido[1',2':3,4]imidazo[1,2-*b*]cinnolin-10-ium tetrafluoroborate (10). Following the general procedure for the Suzuki coupling reaction, starting from compound **6** (70 mg, 0.12 mmol), phenylboronic acid (29 mg, 0.24 mmol), potassium fluoride (29 mg, 0.48 mmol) and [1,1'-bis(diphenylphosphino)-ferrocene]dichloropalladium(II) complex with dichloromethane (1:1) (6 mg, 0.007 mmol), and after purification by flash column chromatography (98:2→95:5 CH_2Cl_2/MeOH), the desired product **10** was obtained in 43% yield (25 mg). M.p: 274–276 °C (decomposition). IR (KBr) ν cm^{-1}: 3452, 1652, 1522, 1491, 1390, 1233, 1084, 764, 702. ^{1}H NMR (500 MHz, DMSO d_6) δ 10.69 (s, 1H), 9.90 (s, 1H), 9.44 (s, 1H), 9.10 (d, *J* = 7.7 Hz, 1H), 9.00–8.75 (m, 3H), 8.43–8.19 (m, 2H), 7.99–7.87 (m, 6H), 7.70–7.58 (m, 3H). ^{13}C NMR (75 MHz, DMSO d_6) δ 146.5, 134.2, 132.0, 131.8, 130.9, 130.6, 129.8, 129.1, 129.0, 128.7, 128.4, 128.2, 126.4, 125.4, 124.7, 124.4, 124.2, 123.9, 123.5, 121.7, 121.5, 117.5, 113.9, 108.7. HRMS (ESI-TOF) for $C_{28}H_{18}N_3^+$ m/z (Calc.): 396.1495, m/z (Found): 396.1495.

14-(4-Methoxyphenyl)dibenzo[*f*,*h*]pyrido[1',2':3,4]imidazo[1,2-*b*]cinnolin-10-ium tetrafluoroborate (11). Following the general procedure for the Suzuki coupling reaction, starting from compound **6** (42 mg, 0.07 mmol), methoxyphenylboronic acid (21 mg, 0.14 mmol), potassium fluoride (17 mg, 0.28 mmol) and [1,1'-bis(diphenylphosphino)-ferrocene]dichloropalladium(II) complex with dichloromethane (1:1) (4 mg, 0.004 mmol), and after purification by flash column chromatography (98:2→95:5 CH_2Cl_2/MeOH), the desired product **11** was obtained in 76% yield (27 mg). M.p: 245–247°C. IR (KBr) ν cm^{-1}: 2957, 2927, 2853, 1608, 1507, 1383, 1253, 1084, 762. ^{1}H NMR (500 MHz, DMSO d_6) δ 10.46 (s, 1H), 9.67 (s, 1H), 9.30 (s, 1H), 8.95 (d, *J* = 7.8 Hz, 1H), 8.70–8.68 (m, 3H), 8.22–8.17 (m, 2H), 7.96–7.71 (m, 6H), 7.20 (d, *J* = 8.3 Hz, 2H), 3.87 (s, 3H). ^{13}C NMR (75 MHz, DMSO d_6) δ 159.7, 146.4, 131.9, 131.7, 130.7, 130.5, 129.8, 129.0, 128.3, 128.0, 127.7, 126.2, 125.3, 124.7, 124.4, 124.1, 123.9, 123.5, 121.4, 120.1, 117.4, 114.4, 113.6, 108.6, 55.0. HRMS (ESI-TOF) for $C_{29}H_{20}N_3O^+$ m/z (Calc.): 426.1601, m/z (Found): 426.1598.

Ligand-DNA binding

Materials. Stock concentrated solutions of ligands were dissolved in DMSO (Aldrich, HPLC grade) and diluted with an aqueous solution to reach concentrations in the 8.3×10^{-6}–1.7×10^{-5} M range. The final solutions contained 5% of DMSO. A 2 mg/mL calf thymus DNA (ctDNA, high molecular weight sodium salt, Aldrich) was prepared in Milli-Q water. For titration purposes a ctDNA of 2.36×10^{-3} mol/per base pair stock solution was prepared in the buffer from the previous solution. This concentration (per pair of bases) was determined by UV-Vis (ε_{260nm}= 13,200 $M^{-1}cm^{-1}$).[29] Small aliquots of this stock DNA solution were added to a rectangular 10 mm path cuvette containing 2.5 or 3.0 mL of the above-mentioned ligand solution. After each addition during titration the content was stirred for about 10 min. The titration reached L/DNA base pair molar ratios of approximately up to 1/35 depending on the association constant of the system.

Instrumentation. Absorption spectra were recorded in a UV-Vis Uvikon 941 (Kontron Instruments) spectrophotometer. Steady-state fluorescence measurements were carried out using a PTI Quanta Master spectrofluorimeter equipped with a Xenon flash lamp as a light source, single concave grating monochromators and Glan–Thompson polarizers in the excitation and emission paths. Detection was allowed by a photomultiplier cooled by a Peltier system. Slit widths were selected at 6–12 nm for both excitation and emission paths and polarizers were fixed at the 'magic angle' conditions. Fluorescence decay measurements were performed on a time-correlated single-photon-counting FL900 Edinburgh Instruments Spectrometer. The excitation sources were a thyratron-gated lamp (nF900) filled with H_2 or a nanoLed (Horiba) emitting at 335 nm. Double concave grating monochromators were employed at both excitation and emission paths. Photons were detected by a red sensitive photomultiplier cooled by another Peltier system. The data acquisition was carried out by using 1024 channels of a multichannel analyzer with a time window width of 100–200 ns depending on the shorter or longer decay times. A total of 10,000 counts in the maximum peak channel were taken for each measurement. The instrumental response function was regularly achieved by measuring the scattering of a Ludox solution. Intensity fluorescence profiles were fitted to multi-exponential decay functions by using the iterative deconvolution method.

Circular dichroism spectra were obtained by using a JASCO-715 spectropolarimeter. Recorded spectra were the average of 3 scans taken at a speed of 50 nm·min^{-1} with a 0.125 s time response. The sensitivity and resolution were fixed at 20 mdeg and 0.5 nm, respectively. When recording the CD spectra for the ligands (ICD) or DNA absorption zones, measurements were performed in 1 cm or 0.1 cm path quartz cells, respectively, at 25 °C.

Live-cell studies. HeLa cells were maintained at 37 °C and 5% CO_2 in Dulbecco's modified Eagle's medium (DMEM) supplemented with 10% foetal calf serum and 100 units/mL penicillin and streptomycin. For live-cell staining, cells were

grown on coverslip-bottom dishes (Nunc™, Thermo Fisher Scientific) and stained by addition of the compound solution 50 mM in DMSO, diluted 1:400 in culture medium (125 uM final). Micrographs were obtained using a Leica SP5 confocal fluorescence microscope equipped with a thermostatic chamber and the following excitation-emission channels (named by the emission colour). Blue: excitation UV diode laser 405 nm, emission filter 420–460 nm. Green: excitation argon laser 488 nm, emission filter 500–570 nm. Red: He/Ne laser 536 nm, emission filter 575–625. Infrared: excitation He/Ne laser 633 nm, emission filter 650–700 nm.

Cytotoxicity experiments were carried out using the standard 3-(4,5-dimethylthiazol-2-yl)-2,5-diphenyltetrazolium bromide (MTT) assay.[30] The cells were seeded into a 24-well plate at a density of 1.5×10^4 cells per well and incubated in medium containing the compound under study at different concentrations for 24 hours. To each well, 100 µL of MTT was added and the plates were incubated at 37 °C for 4 hours to allow MTT to form formazan crystals on reacting with metabolically active cells. The medium with MTT was removed from the wells. Intracellular formazan crystals were dissolved by adding 100 µL of DMSO to each well and the plates were shaken for 10 minutes. The absorbance was recorded using a multiwell plate reader.

Conclusions

A new family of weakly fluorescent dibenzopyridoimidazocinnolinium derivatives whose fluorescence intensity increases significantly upon DNA addition is reported. The synthesis was carried out under mild conditions and in only three steps, which included a Westphal condensation and a Suzuki cross coupling reaction as key steps.

Steady-state and time-resolved fluorescence, along with circular dichroism and molecular modelling techniques, were employed to study derivatives **5**–**11** in the absence and in the presence of ct-DNA. All derivatives interacted with ct-DNA, with binding constants that were in the order of 10^4 M^{-1}. However, among them, ligands **5**, **8**, **10** and **11** are particularly interesting as they exhibited a considerable increase in fluorescence intensity (larger than ×3.5) upon DNA binding. Induced circular dichroism (ICD) spectra confirmed the affinity of these derivatives for double-stranded DNA, which bind to it by intercalation. The sign of the ICD bands together with the Molecular Modelling analysis are consistent with a predominant intercalation process, where the ligand complexed with DNA is oriented with its long axis perpendicular to the base pair pocket axis.

The potential of these compounds for cell staining was investigated in living HeLa cells by confocal microscopy imaging. The results of this analysis showed a remarkable capacity of these azonia cations for active uptake and accumulation by living cells, with complex patterns of intracellular distribution. These cations show a significant increase in their fluorescence intensity upon DNA addition and they are good candidates for use as DNA probes.

Conflicts of interest

There are no conflicts to declare.

Acknowledgements

Financial support from the Spanish Ministerio de Economía y Competitividad (projects CTQ2014-52488-R, CTQ2015-64425-C2-1-R, CTQ2016-80600-P and CTQ2017-85263-R) and Instituto de Salud Carlos III (ISCIII RETIC REDINREN RD16/0009/015 FEDER FUNDS) is gratefully acknowledged. P. B. also thanks the University of Alcalá for his grant. Live-cell studies were performed by ICTS "NANBIOSIS" and its Confocal Microscopy Service: Ciber in Bioengineering, Biomaterials & Nanomedicine (CIBER-BBN), University of Alcala (CAI Medicine Biology).

References

1 (a) E. Pazos, J. Mosquera, M. E. Vázquez and J. L. Mascareñas, *ChemBioChem*, 2011, **12**, 1958; (b) T. Ueno and T. Nagano, *Nature Methods*, 2011, **8**, 642; (c) H. Kobayashi, M. Ogawa, R. Alford, P. L. Choyke and Y. Urano, *Chem. Rev.*, 2010, **110**, 2620.

2 (a) P. M. Pithan, D. Decker, S. I. Druzhinin, H. Ihmels, H. Schönherr and Y. Voß, *RSC Adv.*, 2017, **7**, 10660; (b) D.-L. Ma, H.-Z. He, K.-H. Leung, H.-J. Zhong, D. S.-H. Chan and C.-H. Leung, *Chem. Soc. Rev.,* 2013, **42**, 3427.

3 (a) H. Ihmels and L. Thomas L, in: *Materials science of DNA*, eds. J.-I. Jin and J. Grote, CRC Press, 2011, ch. 3, p. 49; (b) Y. Xie, V. K. Tam and Y. Tor, in *The chemical biology of nucleic acids*, ed. G. Mayer, John Wiley & Sons, Ltd, 2010, ch. 6, p. 115; (c) M. J. Hannon, *Chem. Soc. Rev.*, 2007; **36**, 280.

4 A. Paul and S. Bhattacharya, *Curr. Sci.*, 2012, **102**, 212.

5 (a) A. Granzhan, H. Ihmels and M. Tian, *Arkivoc*, 2015, *vi*, 494; (b) L. Chang, C. Liu, S. He, Y. Lu, S. Zhang, L. Zhao and X. Zeng, *Sens. Actuators B*, 2014, **202**, 483.

6 H. Ihmels, K. Faulhaber, D. Vedaldi, F. Dall'Acqua, and G. Viola, *Photochem. Photobiol.*, 2005, **81**, 1107.

7 K. Bhadra and G. S. Kumar, *Med. Res. Rev.*, 2011, **31**, 821.

8 (a) D. Sucunza, A. M. Cuadro, J. Alvarez-Builla and J. J. Vaquero, *J. Org. Chem.*, 2016, **81**, 10126; (b) A. Granzhan and H. Ihmels, *Synlett*, 2016, **27**, 1775.

9 (a) K. Schaefer, H. Ihmels, E. Porcu and G. Viola, *Chem.-Eur. J.*, 2017, **23**, 370; (b) J. Becher, D. V. Berdnikova, D. Dzubiel, H. Ihmels and P. M. Pithan, *Beilstein J. Org. Chem.*, 2017, **13**, 203; (c) K. Schaefer, H. Ihmels, C. Bohne, K. P. Valente, and A. Granzhan, *J. Org. Chem.*, 2016, **81**, 10942; (d) D. V. Berdnikova, T. M. Aliyeu, T. Paululat, Y. V. Fedorov, O. A. Fedorova and H. Ihmels, *Chem. Commun.*, 2015, **51**, 4906; (e) K. Benner, H. Ihmels, S. Kölsch and P. M. Pithan, *Org. Biomol. Chem.*, 2014, **12**, 1725; (f) R. Bortolozzi, H. Ihmels, L. Thomas, M. Tian and G. Viola, *Chem.–Eur. J.*, 2013, **19**, 8736; (g) K. Faulhaber, A. Granzhan, H. Ihmels, D. Otto, L. Thomas, and S. Wells, *Photochem. Photobiol. Sci.*, 2011, **10**, 1535.

10 (a) C. Norez, C. Jayle, F. Becq and C. Vandebrouck, *Pulm. Pharmacol. Ther.*, 2014, **27**, 38; (b) C. Norez, F. Bilan, A. Kitzis, Y. Mettey and F. Becq, *J. Pharmacol. Exp. Ther.*, 2008,

325, 89; (c) C. Marivingt-Mounir, C. Norez, R. Dérand, L. Bulteau-Pignoux, D. Nguyen-Huy, B. Viossat, G. Morgant, F. Becq, J.-M. Vierfond and Y. Mettey, *J. Med. Chem.*, 2004, **47**, 962.

11 (a) E. Zacharioudakis, T. Caneque, R. Custodio, S. Muller, A. M. Cuadro, J. J. Vaquero, R. Rodriguez, *Bioorg. Med. Chem. Lett.*, 2017, **27**, 203; (b) T. Caneque, A. M. Cuadro, R. Custodio, J. Alvarez-Builla, B. Batanero, P. Gomez-Sal, J. Perez-Moreno, K. Clays, O. Castano, J. L. Andres, T. Carmona, F. Mendicuti and J. J. Vaquero, *Dyes Pigm.*, 2017, **144**, 17; (c) A. Abengozar, B. Abarca, A. M. Cuadro, D. Sucunza, J. Alvarez-Builla and J. J. Vaquero, *Eur. J. Org. Chem.*, 2015, **19**, 4214; (d) G. Marcelo, S. Pinto, T. Cañeque, I. F. A. Mariz, A. M. Cuadro, J. J. Vaquero, J. M. G. Martinho and E. M. S. Maçôas, *J. Phys. Chem. A*, 2015, **119**, 2351; (e) B. Abarca, R. Custodio, A. M. Cuadro, D. Sucunza, A. Domingo, F. Mendicuti, J. Álvarez-Builla and J. J. Vaquero, *Org. Lett.*, 2014, **16**, 3464; (f) T. Cañeque, A. M. Cuadro, J. Alvarez-Builla, J. Pérez-Moreno, K. Clays, O. Castaño, J. L. Andrés and J. J. Vaquero, *Dyes Pigm.*, 2014, **101**, 116; (g) E. Maçôas, G. Marcelo, S. Pinto, T. Cañeque, A. M. Cuadro, J. J. Vaquero and J. M. G. Martinho, *Chem. Commun.*, 2011, **47**, 7374; (h) A. Núñez, B. Abarca, A. M. Cuadro, J. Alvarez-Builla and J. J. Vaquero, *Eur. J. Org. Chem.*, 2011, 1280.

12 (a) X.-L. Sha, J.-Y. Niu, R. Sun, Y.-J. Xub and J.-F. Ge, *Org. Chem. Front.*, 2018, **5**, 555. (b) F. Li, J. Cho, S. Tan and S. Kim, *Org. Lett.*, 2018, **20**, 824. (c) J.-R. Deng, W.-C. Chan, N. C.-H. Lai, B. Yang, C.-S. Tsang, B. C.-B. Ko, S. L.-F. Chan and M.-K. Wong, *Chem. Sci.*, 2017, **8**, 7537.

13 R. M. Suárez, P. Bosch, D. Sucunza, A. M. Cuadro, A. Domingo, F. Mendicuti and J. J. Vaquero, *Org. Biomol. Chem.*, 2015, **13**, 527.

14 P. Bosch, V. García, B. S. Bilen, D. Sucunza, A. Domingo, F. Mendicuti and J. J. Vaquero, *Dyes Pigm.*, 2017, **138**, 135.

15 A. Barbafina, M. Amelia, L. Latterini, G. G. Aloisi and F. Elisei, *J. Phys. Chem. A*, 2009, **113**, 14514.

16 (a) A. Granzhan, H. Ihmels and G. Viola, *J. Am. Chem. Soc.*, 2007, **129**, 1254; (b) A. Granzhan and H. Ihmels, *Org. Lett.*, 2005, **7**, 5119; (c) Z. R. Grabowski and K. Rotkiewicz, *Chem. Rev.* 2003, **103**, 3899.

17 Y. Prostota, O. D. Kachkovsky, L. V. Reis and P. F. Santos, *Dyes Pigm.*, 2013, **96**, 554.

18 K. W. Duncan, R. Chesworth, M. J. Munchhof and L. Jin, PCT Int. Appl. WO 2014100695 A1 20140626, 2014.

19 J. Mendiola, J. A. Rincón, C. Mateos, J. F. Soriano, O. de Frutos, J. K. Niemeier and E. M. Davis, *Org. Process Res. Dev.,* 2009, **13**, 263.

20 M. P. Matia, J. L. García-Navío, J. J. Vaquero and J. Alvarez-Builla, *Liebigs Ann. Chem.*, 1992, 777.

21 M. Tian and H. Ihmels, *Synthesis*, 2009, **24**, 4226.

22 (a) A. M. Brouwer, *Pure Appl. Chem.*, 2011, **83**, 2213; (b) F. Mendicuti and W. L. Mattice, *Polym. Bull.*, 1989, **22**, 557.

23 (a) G. Haberhauer, R. Gleiter and C. Burkhart, *Chem. Eur. J.*, 2016, **22**, 971; (b) D. Li, D. Yu, Q. Zhang, S. Li, H. Zhou, J. Wu and Y. Tian, *Dyes Pigm.*, 2013, **97**, 278; (c) B. Jedrzejewska, M. Pietrzak and J. Paczkowski, *J. Fluoresc.*, 2010, **20**, 73; (d) B. Valeur, In *Molecular fluorescence: Principles and Applications*, Eds. Wiley-VCH: Weinheim, 2001; Chapter 3, p. 62.

24 (a) M. Ardhammar, B. Nordén and T. Kurucsev, In *Circular Dichroism: Principles and Applications*, Berova, N.; Nakanishi, K.; Woody, R. W.; Editors, Eds. Wiley-VCH: Weinheim, 2000; p. 741; (b) W. C. Johnson, In *Circular Dichroism: Principles and Applications*, Berova, N.; Nakanishi, K.; Woody, R. W.; Editors, Eds. Wiley-VCH: Weinheim, 2000; p. 703.

25 (a) M. N. Dehkordia, A.-K. Bordbara, P.Lincolnb and V. Mirkhania, *Spectrochimica Acta Part A*, 2012, **90**, 50; (b) K. Triantafillidi, K. Karidi, O. Novakova, J. Malina, and A. Garoufis, *Dalton Trans.*, 2011, **40**, 472; (c) J. Kypr, I. Kejnovska, D. Renciuk and M. Vorlickova, *Nucleic Acids Res.* 2009, **37**, 1713; (d) K. Karidi, A. Garoufis, N. Hadjiliadis and J. Reedijkb, *Dalton Trans.*, 2005, 728.

26 S. Zhang, Y. Zhu, C. Tu, H. Wei, Z. Yang, L. Lin, J. Ding, J. Zhang and Z. Guo, *J. Inorg. Biochem.*, 2004, **98**, 2099.

27 (a) T. Šmidlehner, I. Piantanida and G. Pescitelli, *Beilstein J. Org. Chem.* 2018, **14**, 84; (b) M. Tian, H. Ihmels and S. Ye, *Org. Biomol. Chem.*, 2012, **10**, 3010; (c) S. Basili, A. Bergen, F. Dall'Acqua, A. Faccio, A. Granzhan, H. Ihmels, S. Moro and G. Viola, *Biochemistry*, 2007, **46**, 12721; (d) B. Nordén and T. Kurucsev, *J. Mol. Recognit.*, 1994, **7**, 141.

28 (a) A. S. Klymchenko, *Acc. Chem. Res.*, 2017, **50**, 366; (b) A. Nakamura and S. Tsukiji, *Bioorg. Med. Chem. Lett.*, 2017, **27**, 3127; (c) Z. Ma, Y. Lin, Y. Cheng, W. Wu, R. Cai, S. Chen, B. Shi, B. Han, X. Shi, Y. Zhou, L. Du and M. Li, *J. Med. Chem.*, 2016, **59**, 2151; (d) A. S. Klymchenko and Y. Mely, *Prog. Mol. Biol. Transl. Sci.*, 2013, **113**, 35; (e) T. Zal, M. A. Zal, C. Lotz, C. J. Goergen and N. R. Gascoigne, *Traffic*, 2006, **7**, 1607; (f) S. Bolte, C. Talbot, Y. Boutte, O. Catrice, N. D. Read and B. Satiat-Jeunemaitre; *J. Microsc.*, 2004, **214**, 159.

29 A. W. McConnaughie and T. C. Jenkins, *J. Med. Chem.*, 1995, **38**, 3488.

30 T. Mosmann, *J. Immunol. Methods*, 1983, **65**, 55.

